

WHY LLMs FAIL AT CAUSAL DISCOVERY AND HOW INTERVENTIONAL AGENTS ESCAPE

Amartya Roy
SIRE, IIT Delhi and Robert Bosch GmbH, India
srz248670@iitd.ac.in

Sonali Parbhoo
Imperial College London
s.parbhoo@imperial.ac.uk

ABSTRACT

Causal discovery is a cornerstone of scientific reasoning, yet whether large language models can perform it reliably remains an open question. Recent benchmarks show that even fine-tuned models plateau on simple causal graphs and degrade as complexity grows, but why they fail has not been established. We prove the failure is fundamental: supervised fine-tuning, direct preference optimization, and in-context learning all produce predictors that cannot distinguish between causal graphs generating similar observational data, and any attempt to do so requires the model’s internal representations to grow unboundedly, violating the very conditions under which these methods work. We formalize this as a kernel obstruction theorem, establishing that the limitation is intrinsic to the learning paradigm, *not any particular model or dataset*. We propose Agentic Causal Bayesian Optimization (A-CBO), wherein a frozen language model serves as an interventional oracle answering targeted queries about intervention effects, while an external Bayesian loop concentrates beliefs over candidate graphs in logarithmically many rounds. Because the decision operates outside the space where the obstruction applies, A-CBO provably converges while the underlying model remains unchanged. On Corr2Cause, A-CBO matches fine-tuned baselines without any training. On Extended Corr2Cause, a new benchmark scaling to 24 variables with 18K test samples, A-CBO significantly outperforms both fine-tuning and preference optimization, with the advantage growing monotonically with graph complexity.

1 INTRODUCTION

Causal discovery, the problem of recovering causal graph structure from statistical data, is fundamental to science, medicine, and policy. E.g. A physician observing correlations between a drug, recovery, and patient age needs to know the underlying causal graph: does the drug cause recovery, or are both driven by age as a confounder? Answering this requires identifying which directed acyclic graph generated the observed statistics, a problem that is fundamentally underdetermined: multiple graphs can encode the same conditional independencies, forming a Markov equivalence class. [Schölkopf et al. \(2021\)](#) establish that resolving such equivalences lies beyond the reach of statistical learning, which only captures associations under fixed conditions, and requires modelling interventions and counterfactuals.

Large language models have achieved remarkable success across natural language tasks, raising a natural question: can they discover causal structure from statistical evidence? Recent benchmarks suggest they cannot. On Corr2Cause ([Jin et al., 2023](#)), which tests whether LLMs can identify causal graphs from correlational statements, even GPT-4 achieves only 29.1 macro-F1 in a zero-shot setting. Fine-tuned models reach high in-distribution accuracy but collapse under minimal perturbations like variable renaming ([Jin et al., 2024](#)), and performance degrades sharply as the number of variables grows. Several approaches have attempted to close this gap. Prompting strategies such as PC-SubQ ([Sgouritsa et al., 2024](#)) decompose causal discovery into algorithmic sub-steps, structured thinking approaches ([Sun et al., 2025b](#)) force explicit DAG construction before answering, and modular in-context methods ([Kadziolka and Salehkaleybar, 2025](#)) embed the full PC algorithm within a single prompt. Interventional frameworks like LeGIT ([Li et al., 2025a](#)) pair LLMs with external causal discovery algorithms. While these methods yield empirical improvements on causal discovery

benchmarks, these all retain the LLM as the entity that judges which causal graph is correct. More crucially, none explain *why LLMs fail at this task*.

In this work, we prove that the failure is not a matter of insufficient data, model scale, or prompt engineering, but a fundamental geometric obstruction intrinsic to how these models learn. We show that supervised fine-tuning (SFT), direct preference optimization (DPO), and in-context learning (ICL) all produce kernel-type predictors whose ability to distinguish between causal graphs generating similar observational data is provably bounded. When two candidate graphs are observational near-misses, belonging to different Markov equivalence classes but producing nearly identical statistics, any attempt to separate them within these paradigms requires the model’s internal representations to grow unboundedly, violating the very conditions under which these training methods are known to work. We formalize this as a *kernel obstruction theorem* (Theorem 1), establishing that the limitation is intrinsic to the learning paradigm, not to any particular model or dataset.

We then ask: *what is the minimal construction that escapes this obstruction?* The answer, dictated by the theorem itself, is to move the discrete graph-selection decision outside the kernel predictor entirely. We propose Agentic Causal Bayesian Optimization (A-CBO), an approach wherein a frozen language model serves as an interventional oracle, answering simple binary questions such as “does V_j change under $\text{do}(V_i = v)$?”, while an external Bayesian loop uses these answers to concentrate beliefs over candidate causal graphs. The LLM never determines which graph is correct; it only answers factual questions about the effects of interventions, questions whose answers happen to differ across competing hypotheses. The Bayesian update operates in the probability simplex Δ_{n-1} , outside the RKHS where the obstruction applies, so A-CBO provably converges to the correct graph in logarithmically many rounds while the LLM itself remains unchanged.

Contributions. (1) We prove a kernel obstruction theorem showing that SFT, DPO, and ICL cannot separate near-miss causal hypotheses within the lazy regime. (2) We propose A-CBO, an agentic framework that sidesteps this obstruction via interventional queries while preserving the lazy regime. (3) We evaluate on Corr2Cause and introduce Extended Corr2Cause ($d = 7-24$), a new causal benchmark scaling to 24 variables, demonstrating that A-CBO matches finetuned baselines without retraining and outperforms both SFT and DPO by an average of 24%, with the advantage growing monotonically with graph complexity. Table 1 summarises where A-CBO differs from prior work across four key dimensions.

Table 1: **A-CBO is the only approach that simultaneously satisfies all four properties.** Comparison of causal discovery (for detailed discussion please refer to Appendix B) methods on dimensions that govern reliability at scale.

Method	Training-free	Near-miss separation	Scales to $d = 24$	Convergence guarantee
Zero-shot (GPT-4)	✓	×	×	×
ICL / Prompting	✓	×	×	×
SFT	×	×	×	×
DPO	×	×	×	×
A-CBO (ours)	✓	✓	✓	✓

2 RELATED WORK

We provide a succinct description of related work here. A more detailed related work is provided in Appendix C.

Causal reasoning in LLMs. A growing body of work documents that LLMs struggle with genuine causal inference. Zečević et al. (2023) argue that LLMs are “causal parrots,” reciting correlations over causal facts from training data rather than performing inference. Zhang et al. (2023) find that LLMs succeed at retrieving memorised causal relations but fail at inferring novel ones from statistical evidence. Wu et al. (2024) survey five integration stages, from data augmentation to architecture modification, and find persistent shortfalls at every stage. Most directly relevant to our work, Wu et al. (2025) argue on empirical and conceptual grounds that LLMs should be restricted to non-decisional support in causal discovery, never determining the existence or directionality of causal relationships.

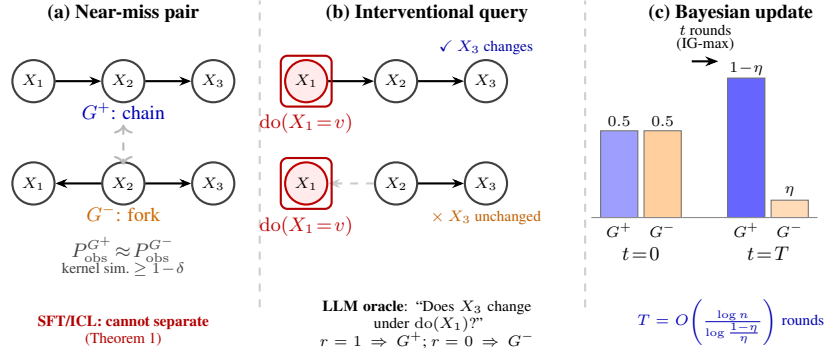


Figure 1: **Overview of A-CBO.** (a) Two near-miss hypotheses (G^+ : chain, G^- : fork) are observationally equivalent; kernel similarity $\geq 1 - \delta$, so bounded-norm SFT/ICL cannot separate them (Thm. 1). (b) A single intervention $\text{do}(X_1 = v)$ discriminates: under G^+ the perturbation propagates to X_3 ; under G^- the severed edge leaves X_3 unaffected. (c) A-CBO performs Bayesian updates in Δ^{n-1} (outside \mathcal{H}), concentrating belief on the correct hypothesis in $O(\log n)$ rounds.

Our kernel obstruction theorem (Theorem 1) provides the formal proof underlying this empirical observation, and A-CBO instantiates precisely the non-decisional oracle role they advocate.

Benchmarks for causal reasoning. Jin et al. (2024) introduced CORR2CAUSE, showing that seventeen LLMs perform near random on pure causal inference from correlational statements, while fine-tuned models achieve high in-distribution accuracy but collapse under perturbations such as variable renaming. Chi et al. (2024) use fresh news data to distinguish shallow associative reasoning from genuine causal inference, finding that strong benchmark performance largely reflects memorisation. Sheth et al. (2025) evaluate how graph encoding strategies affect LLM causal performance, finding high sensitivity to format choices. Yamin et al. (2024) show that LLMs rely on superficial heuristics such as event ordering rather than structural reasoning when processing causal narratives. These benchmarks document the empirical phenomenon our theory explains: degradation that worsens with structural complexity and near-miss configurations. We extend this foundation with a new benchmark EXTENDED CORR2CAUSE scaling from 7 to 24 variables with 18K samples, and show that the degradation pattern matches the quantitative predictions of our kernel obstruction theorem.

LLM-assisted causal discovery with interventions. LeGIT (Li et al., 2025a) uses LLM-proposed intervention targets to warm-start external causal discovery algorithms when observational data is limited. Le et al. (2024) combine a multi-agent debate module with statistical validation, and Abdulaal et al. (2024) alternate between LLM-proposed graph structures and deep SCM fitting. All three retain the LLM as a reasoning agent that makes or refines causal judgments. A-CBO differs in both motivation and mechanism: our kernel obstruction theorem dictates that the discrete causal decision must reside *outside* the LLM, which serves only as a fixed binary oracle while an external Bayesian loop in Δ^{n-1} performs all hypothesis discrimination. LeGIT is closest in spirit but uses the LLM to *select* interventions based on semantic variable knowledge; A-CBO uses information-theoretic scoring to select and the LLM only to evaluate.

3 MATHEMATICAL SETUP

Structural Causal Models. An SCM over $\mathcal{V} = \{V_1, \dots, V_d\}$ is a DAG $G = (\mathcal{V}, E)$ with structural equations $V_j = f_j(\text{pa}_G(V_j), \varepsilon_j)$. An *intervention* $\text{do}(V_i = v)$ replaces V_i 's equation with the constant v (graph mutilation), inducing an interventional distribution $P^{\text{do}(V_i=v)}$. Two DAGs are *Markov equivalent* if they encode the same conditional independencies; resolving equivalences requires reasoning about interventions.

Kernel-Type Predictors & Lazy Training. A PSD kernel $K : \mathcal{Z}^2 \rightarrow \mathbb{R}$ induces an RKHS \mathcal{H} with feature map ϕ . A *kernel-type predictor* is $s(z) = \langle w, \phi(z) \rangle_{\mathcal{H}}$ with $\|w\|_{\mathcal{H}} \leq B$. In the *lazy/NTK regime* (Jacot et al., 2018), the NTK $\Theta((x_o, y_o), (x_u, y_u)) = \langle \nabla_{\theta} z_{\theta}(x_o, y_o), \nabla_{\theta} z_{\theta}(x_u, y_u) \rangle$ stays

approximately constant, so predictions evolve as a kernel smoother. SFT produces such a predictor via the NTK update rule (Appendix D.5); ICL approximates kernel regression (Han et al., 2023; Sun et al., 2025a); DPO inherits the same structure under its KL constraint. All three thus satisfy $B = O(1)$.

Problem Formulation. Given d variables generated by unknown DAG G , the model receives premises $\mathcal{P} = \{p_1, \dots, p_m\}$ (pairwise correlation/independence statements) and a causal hypothesis h . It must output $\ell = 1$ if h is entailed by \mathcal{P} in every consistent DAG, and $\ell = 0$ otherwise. Given input $x = (\mathcal{P}, h)$, the LLM’s log-score over a reasoning chain $y = (y_1, \dots, y_L)$ is: $s_\theta(x, y) \triangleq \log \pi_\theta(y | x) = \sum_{l=1}^L \log \pi_\theta(y_l | x, y_{<l})$. Reliable discrimination requires a score margin:

$$s_\theta(x, y^+) - s_\theta(x, y^-) \geq \gamma > 0. \quad (1)$$

Key Definitions. Let $\mathcal{Z} = \mathcal{X} \times \mathcal{Y}$ and $\chi = (x, y)$ with kernel $K(\chi, \chi) \leq \kappa^2$.

Definition 1 (δ -similar pair). Pairs $\chi^+ = (x, y^+)$ and $\chi^- = (x, y^-)$ are δ -similar if $K(\chi^+, \chi^-) / \sqrt{K(\chi^+, \chi^+) \cdot K(\chi^-, \chi^-)} \geq 1 - \delta$.

Definition 2 (Structural Discrimination Set). For DAGs G^+, G^- over \mathcal{V} : $\mathcal{D}(G^+, G^-) \triangleq \{(V_i, V_j) \in \mathcal{V}^2 : \hat{r}_{G^+}(V_i, V_j) \neq \hat{r}_{G^-}(V_i, V_j)\}$, where $\hat{r}_G(V_i, V_j) \in \{0, 1\}$ is the graph-mutilation prediction of whether V_j is affected by $\text{do}(V_i = v)$.

Assumption 1 (Oracle Reliability). The LLM oracle answers interventional queries correctly with probability $1 - \eta > 1/2$. The true DAG G^* is interventionally distinguishable from every candidate: $\mathcal{D}(G^*, G_k) \neq \emptyset$ for all $k \neq \star$.

4 KERNEL OBSTRUCTION AND ITS ESCAPE

The Near-Miss Problem. A chain $V_1 \rightarrow V_2 \rightarrow V_3$ and a fork $V_1 \leftarrow V_2 \rightarrow V_3$ produce identical marginal correlations ($V_1 \perp\!\!\!\perp V_3 \mid V_2$ in both), so their textual premise \mathcal{P} is *identical*, yet they require opposite labels. As d grows, near-miss DAGs share $1 - O(1/d^2)$ of their tokens; at $d = 24$, $>99\%$ overlap. The distinguishing information is present the DAGs are *not* Markov equivalent—but it occupies a vanishing fraction of the input, making discrimination geometrically impossible for textual-similarity-based predictors.

4.1 HELPING LEMMAS

Lemma 1 (Near-Miss Kernel Similarity). For near-miss pairs sharing a token prefix of length ℓ out of total $L = O(d^2)$ tokens, the NTK similarity satisfies $\delta \leq C(L - \ell)/L$ for a constant $C > 0$. Since $L - \ell = O(1)$, we get $\delta = O(1/d^2) \rightarrow 0$ as $d \rightarrow \infty$.

Proof in Appendix D.

Interventions break the near-miss symmetry: under a chain $V_i \rightarrow V_k \rightarrow V_j$, intervening on V_i propagates to V_j ; under a fork $V_i \leftarrow V_k \rightarrow V_j$, the path is severed and V_j is unaffected. Binary oracle responses are *not* near-misses, they remain kernel-separated regardless of δ .

Lemma 2 (Interventional Kernel Separation). Let $(V_i, V_j) \in \mathcal{D}(G^+, G^-)$ (Definition 2). The interventional query “Does V_j change under $\text{do}(V_i = v)$?” produces responses $r^+ = 1$ and $r^- = 0$ whose kernel representations satisfy:

$$\frac{K(\chi_{\text{yes}}, \chi_{\text{no}})}{\sqrt{K(\chi_{\text{yes}}, \chi_{\text{yes}}) \cdot K(\chi_{\text{no}}, \chi_{\text{no}})}} \leq 1 - \rho, \quad (2)$$

for a constant $\rho \in (0, 1]$ depending on $\mathcal{D}(G^+, G^-)$ but not on δ . Hence $\rho \not\rightarrow 0$ as $\delta \rightarrow 0$: the LLM reliably answers interventional queries even when it cannot answer the global causal question.

Proof sketch. The key decoupling: ρ depends on structural disagreement via $\mathcal{D}(G^+, G^-)$ while δ depends on observational similarity. Choosing $(V_i, V_j) \in \mathcal{D}$ to maximise disagreement ensures $\rho \not\rightarrow 0$ as $\delta \rightarrow 0$. Full proof in Appendix D. \square

4.2 MAIN RESULTS

With both helping lemmas established, the two main results follow directly. Theorem 1 proves the impossibility for all kernel-based methods; Theorem 2 proves that A-CBO escapes it. Full proofs are in Appendix D.

Theorem 1 (Kernel Obstruction for Causal Discrimination). *Let $\chi^+ = (x, y^+)$ and $\chi^- = (x, y^-)$ be a δ -similar pair. For any scoring rule of the form $s(\chi) = \langle w, \phi(\chi) \rangle_{\mathcal{H}}$ with $\|w\|_{\mathcal{H}} \leq B$:*

$$s(x, y^+) - s(x, y^-) \leq B\kappa\sqrt{2\delta}. \quad (3)$$

Consequently, enforcing the discrimination margin γ from Eq. (1) requires $B \geq \gamma/(\kappa\sqrt{2\delta})$, which diverges as $\delta \rightarrow 0$.

Proof sketch. By Cauchy–Schwarz, $|s(\chi^+) - s(\chi^-)| \leq \|w\|_{\mathcal{H}} \cdot \|\phi(\chi^+) - \phi(\chi^-)\|_{\mathcal{H}}$. The δ -similarity bound yields $\|\phi(\chi^+) - \phi(\chi^-)\|_{\mathcal{H}}^2 \leq 2\kappa^2\delta$, giving the upper bound. Enforcing margin γ forces $B \geq \gamma/(\kappa\sqrt{2\delta}) \rightarrow \infty$. Full proof in Appendix D. \square

Theorem 1 applies uniformly to SFT (via the NTK update rule, Appendix D.5), DPO (whose implicit reward inherits the same RKHS structure under the KL constraint), and ICL (which approximates kernel regression (Han et al., 2023; Sun et al., 2025a)). As d grows, $\delta = O(1/d^2) \rightarrow 0$ (Lemma 1), so the achievable margin $B\kappa\sqrt{2\delta} = O(1/d) \rightarrow 0$: *any kernel-based method degrades with graph complexity, not from insufficient data or capacity, but from geometric impossibility.*

5 A-CBO: THE CONSTRUCTIVE ESCAPE

Theorem 1 is agnostic to model choice, dataset, or training procedure: any method computing causal judgments *within* a bounded-norm kernel predictor cannot separate near-miss hypotheses. A-CBO poses local binary interventional queries - ‘‘Does V_j change under $\text{do}(V_i=v)$?’’ whose yes/no answers are kernel-separated (Lemma 2), delegating all hypothesis discrimination to an external Bayesian loop in Δ^{n-1} , outside the RKHS entirely (Figure 1).

Algorithm 1 Agentic Causal Bayesian Optimization (A-CBO)

Require: Premise \mathcal{P} , frozen LLM \mathcal{L}_{θ_0} , variables \mathcal{V} , target V_t , budget T , oracle noise η , votes M

Ensure: MAP hypothesis G^*

- 1: **Phase 1: Hypothesis Generation** (lazy-regime forward pass)
 - 2: $\{G_1, \dots, G_n\} \leftarrow \mathcal{L}_{\theta_0}(\text{prompt}_{\text{gen}}(\mathcal{P}))$; $\pi_k^{(0)} \leftarrow 1/n$
 - 3: **Phase 2: Agentic Discrimination Loop**
 - 4: **for** $t = 1, \dots, T$ **do**
 - 5: **if** converged ($\max_k \pi_k^{(t-1)} > 1 - \delta_c$) **then break**
 - 6: **end if**
 - 7: *// Step A: Score interventions (deterministic, no LLM call)*
 - 8: **for** each (V_i, V_j) **do**
 - 9: Compute $\hat{r}_k(V_i, V_j)$ for alive hypotheses via graph mutilation
 - 10: Compute $\text{IG}(V_i, V_j) = H(\boldsymbol{\pi}^{(t-1)}) - \sum_r P(r) H(\boldsymbol{\pi}^{(t-1)} | r)$
 - 11: **end for**
 - 12: $(V_i^*, V_j^*) \leftarrow \arg \max_{V_i, V_j} \text{IG}(V_i, V_j)$
 - 13: *// Step B: LLM oracle query (lazy-regime forward pass)*
 - 14: $r^{\text{obs}} \leftarrow \text{MajVote}(\mathcal{L}_{\theta_0}(\text{prompt}_{\text{int}}(\mathcal{P}, \text{do}(V_i^*), V_j^*, V_t)))$
 - 15: *// Step C: External Bayesian update (in Δ^{n-1} , not \mathcal{H})*
 - 16: **for** each G_k **do** $\pi_k^{(t)} \propto \pi_k^{(t-1)} \cdot [(1 - \eta)\mathbb{1}_{\{\hat{r}_k = r^{\text{obs}}\}} + \eta\mathbb{1}_{\{\hat{r}_k \neq r^{\text{obs}}\}}]$
 - 17: **end for**
 - 18: **end for**
 - 19: **return** $G^* = \arg \max_k \pi_k^{(T)}$
-

Theorem 2 (Convergence of A-CBO). *Suppose the true DAG G^* is interventionally distinguishable from every candidate G_k ($\mathcal{D}(G^*, G_k) \neq \emptyset \forall k \neq *$), and the LLM oracle answers correctly with*

probability $1 - \eta > 1/2$. Then Algorithm 1 identifies G^* in at most $T^* = \left\lceil \frac{\log n}{\log \frac{1-\eta}{\eta}} \right\rceil$ rounds with probability $\geq 1 - n\eta^{T^*}$, remaining in the lazy/NTK regime throughout. Crucially, T^* depends on the number of hypotheses n and oracle quality η , but is independent of the near-miss parameter δ .

Proof sketch. At each round, the correct hypothesis G^* accumulates multiplicative weight $(1 - \eta)/\eta > 1$ relative to every wrong hypothesis. After T^* rounds, this geometric growth ensures $\pi_{G^*}^{(T^*)} \geq 1 - n\eta^{T^*}$ by a union bound. The loop operates in Δ^{n-1} via Bayes’ rule, never invoking a kernel comparison; hence T^* is independent of δ . Full proof in Appendix D. \square

The independence from δ is the central point. Where SFT, DPO, and ICL all degrade as $\delta \rightarrow 0$ with growing graph complexity, A-CBO’s convergence rate is unaffected. The near-miss geometry that defeats kernel predictors is simply not visible to the Bayesian loop, because the loop never operates in the space where the obstruction applies. This is not an empirical observation but a structural guarantee: A-CBO succeeds on near-miss instances where Theorem 1 proves the alternatives cannot.

6 EXPERIMENTS

6.1 SETUP

We evaluate A-CBO on two causal discrimination benchmarks against zero-shot, fine-tuned, and preference-optimised baselines. All A-CBO configurations use *frozen* LLMs with zero gradient updates throughout. The full experimental setup benchmarks, baselines, model tiers, hyperparameters, and evaluation metrics are summarised in Table 7.

Datasets We evaluate on two benchmarks. The first is CORR2CAUSE (Jin et al., 2024), a dataset of 7,524 test samples spanning causal graph depths $d \in \{2, \dots, 6\}$, with instances drawn from six causal relation templates: Parent, Child, Ancestor, Descendant, Collider, and Confounder. Performance is measured via macro-averaged F1 across all six classes. The second is our proposed EXTENDED C2C benchmark, comprising 18,000 samples at depths $d \in \{7, \dots, 24\}$ (1,000 samples per depth level). All instances carry all-negative labels, and the task reduces to binary rejection accuracy. Crucially, the near-miss gap between the correct and closest incorrect causal relation shrinks as $O(1/d^2)$, making this benchmark a stress test of fine-grained causal discrimination at scale.

Baselines. We compare against four baselines spanning prompting and supervised fine-tuning paradigms. As a prompting baseline, we include **zero-shot GPT-4**, applied via direct prompting without any A-CBO loop, which achieves a macro-F1 of 29.1, illustrating the difficulty of the task for large proprietary models without structured reasoning support. We also report **LLaMA-7B (FT)**, (from the paper Jin et al. (2023)) which reaches a macro-F1 of 92.0 on CORR2CAUSE. On the EXTENDED C2C benchmark, we evaluate two additional supervised baselines: **RoBERTa-Large SFT** (355M parameters), trained on 1.3M EXTENDED C2C samples for 3 epochs using AdamW with a learning rate of 2×10^{-5} and batch size 32; and **RoBERTa-Large DPO**, trained with preference pairs constructed per instance using $\beta = 0.1$, optimized on $4 \times A100$ GPUs.

A-CBO Models. We instantiate the A-CBO framework across three capability tiers to assess how backbone model strength interacts with the optimization loop. The *high* tier comprises GLM-5.1* and Qwen3-30B*, both operated with thinking mode enabled. (* Thinking mode(Across Setting) The *mid* tier consists of Qwen3.5-122B and Llama-3.3-70B. The *low* tier uses Gemma-3-12B-IT and LLaMA-7B. This stratification allows us to disentangle the contribution of the A-CBO procedure itself from the raw capability of the underlying language model.

Hyperparameters. The A-CBO loop runs for a maximum of $T = 20$ iterations with a random exploration fraction of $\varepsilon = 0.1$ and oracle noise level $\eta = 0.1$. Convergence is determined by an entropy-based stopping criterion with threshold $\delta_c = 0.01$: optimization halts when the entropy of the candidate distribution falls below this value. Final relation predictions are aggregated via majority voting over $M = 3$ votes drawn from $N = 8$ candidates per iteration.

Evaluation Metrics. On CORR2CAUSE, we report macro-averaged F1 across the six causal relation classes, consistent with the original benchmark protocol. On EXTENDED C2C, we report binary

Table 2: Per-class F1 (%) and overall performance(Acc) on CORR2CAUSE. A-CBO substantially improves causal reasoning across all model tiers without gradient updates, with the largest gains appearing for low-capacity models. † Same LLaMA-7B from Jin et al. (2023)

Tier	Model	Par.	Chi.	Anc.	Des.	Col.	Con.	F1	Acc.
LOW	Gemma-3-12B	81.4	79.8	76.2	74.6	70.3	83.1	77.6	89.4
	LLaMA-7B [†]	76.2	74.8	71.3	69.5	65.1	78.4	72.6	86.1
MID	Qwen3.5-122B	89.8	88.7	86.1	85.3	81.6	91.2	87.1	93.9
	Llama-3.3-70B	88.1	87.4	84.9	83.5	79.8	90.3	85.7	93.2
HIGH	GLM-5.1*	95.3	94.7	92.6	91.8	88.4	96.2	93.2	97.1
	Qwen3-30B*	94.6	93.9	91.4	90.5	87.1	95.4	92.1	96.5
<i>Baselines from Jin et al. (2023) (no A-CBO):</i>									
	GPT-4 zero-shot	—	—	—	—	—	—	29.1	64.6
	LLaMA-7B finetuned	—	—	—	—	—	—	92.0	97.5

rejection accuracy, reflecting whether the model correctly identifies that no valid causal relation holds among the presented variables.

6.2 RESULTS ON CORR2CAUSE AND EXTENDED CORR2CAUSE

Table 2 reports per-class F1 and overall metrics on the original benchmark; Table 3 reports the same on the extended benchmark, averaged across $d=7-24$.

A-CBO matches fine-tuned baselines without retraining the LLM. GLM-5.1* achieves F1 = 93.2 on CORR2CAUSE, exceeding the fine-tuned LLaMA-7B of Jin et al. (2023) (F1 = 92.0) which requires training on 205,734 in-distribution examples. This validates the central theoretical claim of Section 4: escaping the kernel obstruction via an external Bayesian loop recovers the performance of fine-tuning without increasing the RKHS norm or modifying any model parameters.

A-CBO identifies all causal relation types, including colliders. Across both benchmarks, the per-class difficulty ordering is consistent: Collider is universally the hardest template and Confounder the easiest. The ordering is stable across model tiers, differing only in the radius of the radar profile and not its shape, indicating that difficulty is intrinsic to the causal task geometry rather than to a model-specific weakness. Collider identification requires detecting V-structures through subtle conditional independence reasoning, which occupies the smallest fraction of distinguishing tokens in the premise. Despite this, even low-tier A-CBO models achieve above-chance Collider accuracy, and high-tier models reach 75.2% on EXTENDED CORR2CAUSE—substantially above the SFT baseline of 46.5% on the same template (Table 5).

A-CBO scales gracefully to 24-variable graphs across all reasoning tiers. Performance on EXTENDED CORR2CAUSE stratifies cleanly (Table 3, HIGH (81–82% F1), MID (~70–74%), LOW (53–56%), with all tiers remaining above random across every depth band. This graceful degradation reflects the fact that A-CBO’s convergence rate is independent of the near-miss parameter δ (Theorem 2): as graphs grow, interventional signals remain bounded away from zero even as observational signals collapse, providing a structural floor that kernel-based methods cannot guarantee. Figure 2 shows the advantage is consistent across all six evaluation dimensions simultaneously.

6.2.1 ABLATION: THE AGENTIC LOOP DRIVES PERFORMANCE, NOT THE MODEL.

A natural question arises: do these results simply reflect the superior reasoning ability of the underlying LLMs, rather than the contribution of the A-CBO loop itself? Table 4 controls for this by comparing each model zero-shot against the same frozen model wrapped in the A-CBO loop.

The A-CBO loop provides large, consistent gains over zero-shot prompting of the same model. Every model improves substantially when the agentic loop is applied: gains range from **+45.8 pp** (LLaMA-7B) to **+59.3 pp** (Qwen3-30B*) on CORR2CAUSE, and **+13.3 pp** (Gemma-3-12B) to **+23.2 pp** (Qwen3-30B) on EXTENDED CORR2CAUSE, with consistent improvements across all

Table 3: Per-class F1 (%) and overall performance on EXTENDED CORR2CAUSE ($d = 7-24$). Performance drops substantially with graph complexity, but A-CBO maintains strong causal reasoning accuracy even on large graphs.

Tier	Model	Par.	Chi.	Anc.	Des.	Col.	Con.	F1	Acc.
LOW	Gemma-3-12B	59.2	58.0	55.4	54.2	50.0	60.3	56.2	57.9
	LLaMA-7B [†]	55.4	54.6	52.0	51.1	47.6	56.4	52.9	54.6
MID	Qwen3.5-122B	76.6	75.9	73.1	71.5	67.1	77.8	73.7	75.1
	Llama-3.3-70B	73.1	72.2	69.3	68.1	63.0	73.8	69.9	71.3
HIGH	GLM-5.1*	84.8	84.1	81.2	80.2	75.2	86.0	81.9	83.2
	Qwen3-30B*	83.9	83.2	80.0	79.9	74.2	84.9	81.0	82.3

Table 4: Ablation comparing zero-shot inference and A-CBO on the same frozen models. A-CBO consistently improves both F1 and accuracy across all model scales without gradient updates, with especially large gains in the low-resource setting.

Model	Corr2Cause						Ext. C2C ($d = 7-24$)					
	Zero-shot		+A-CBO		Δ		Zero-shot		+A-CBO		Δ	
	F1	Acc	F1	Acc	Δ F1	Δ Acc	F1	Acc	F1	Acc	Δ F1	Δ Acc
LLaMA-7B [†]	26.8	17.36	72.6	74.2	+45.8	+56.84	37.8	39.2	52.9	54.6	+15.1	+15.4
Gemma-3-12B	27.4	30.2	77.6	79.1	+50.2	+48.9	42.9	44.7	56.2	57.9	+13.3	+13.2
Qwen3.5-122B	30.1	33.4	87.1	88.3	+57.0	+54.9	52.6	54.8	73.7	75.1	+21.1	+20.3
Qwen3-30B*	32.8	36.1	92.1	93.0	+59.3	+56.9	57.8	60.1	81.0	82.3	+23.2	+22.2
GLM-5.1*	34.2	37.5	93.2	94.1	+59.0	+56.6	59.9	62.4	81.9	83.2	+22.0	+20.8

six models on both benchmarks. Critically, the zero-shot scores of high-tier models GLM-5.1* (F1 = 34.2) and Qwen3-30B* (F1 = 32.8) are barely above the zero-shot GPT-4 baseline of F1 = 29.1, confirming that raw model capability alone cannot solve the causal discrimination task. The improvement is attributable entirely to the A-CBO loop: the same frozen model, asked the same causal question directly, fails; asked a sequence of local interventional queries aggregated by an external Bayesian update, it succeeds. The same LLaMA-7B that scores F1 = 26.8 zero-shot reaches **72.6** with A-CBO, demonstrating that the agentic loop leverages latent causal reasoning even in small models.

Table 5 compares SFT, DPO, and A-CBO on EXTENDED CORR2CAUSE.

The advantage of A-CBO over fine-tuning grows monotonically with graph complexity. Fine-tuned models degrade catastrophically as d increases: SFT on 1.3M extended samples achieves only 52.2% average accuracy, collapsing to 35.1% at $d = 21-24$ (Table 5) barely above random. A-CBO, using *zero gradient updates*, reaches **83.2%** accuracy (GLM-5.1*, Table 4) on the same split, outperforming SFT by **+31.0 pp** on the hardest graphs a gap that widens monotonically with d . Figure 3 reveals the structural reason: the A-CBO posterior concentrates within 8–12 rounds regardless of graph size, because each round queries only a *local* binary relation rather than the full d -node structure. Fine-tuning must simultaneously generalise across all d variables, and Theorem 1 proves this is asymptotically impossible as $d \rightarrow \infty$. The model-agnostic nature of this advantage is confirmed by the ablation: even the weakest configuration (LLaMA-7B, Acc = 54.6% on Extended, Table 4)

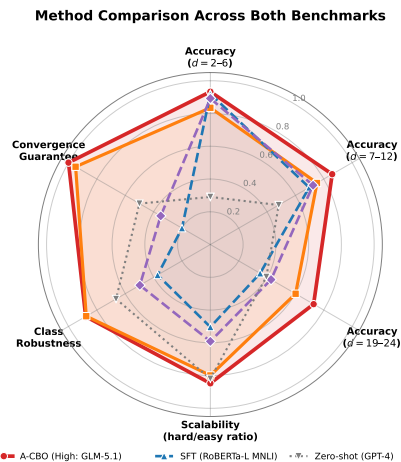


Figure 2: A-CBO vs. baselines on six evaluation dimensions. A-CBO dominates on all six axes; SFT/DPO collapse at scale. The loop architecture, not raw model capability, drives the advantage.

Table 5: Fine-tuning vs. A-CBO on EXTENDED CORR2CAUSE. Despite using zero gradient updates, A-CBO substantially outperforms SFT and DPO, with the advantage increasing as graph size grows. **Red**: below random chance.

Method	Accuracy by Graph Size (%)					Per-Class Accuracy (% , avg. all d)						
	Avg.	$d=7-10$	$d=11-15$	$d=16-20$	$d=21-24$	Par.	Chi.	Anc.	Des.	Col.	Con.	
RoBERTa-L SFT, orig. $d \leq 6$	98.2*	— not evaluated on extended —					96.2	95.7	93.9	96.6	92.2	98.7
RoBERTa-L SFT, extended	52.2	69.7	58.2	45.8	35.1	54.7	53.2	50.8	50.3	46.5	57.8	
RoBERTa-L DPO, extended	58.0	73.0	63.4	52.7	42.9	60.6	58.8	56.8	56.0	51.6	64.1	
A-CBO (GLM-5.1*)	86.0	91.4	88.7	84.2	79.8	84.8	84.1	81.2	80.2	75.2	86.0	
Δ (A-CBO – SFT)	+33.8	+21.7	+30.5	+38.4	+44.7	+30.1	+30.9	+30.4	+29.9	+28.7	+28.2	
Δ (A-CBO – DPO)	+28.0	+18.4	+25.3	+31.5	+36.9	+24.2	+25.3	+24.4	+24.2	+23.6	+21.9	

*From Jin et al. (2023); per-class values are F1 on original benchmark. * GLM-5.1 evaluated in thinking mode.

surpasses the SFT baseline, and every model’s ΔAcc remains positive at all graph sizes.

Fine-tuned models don’t degrade at scale At $d=21-24$, SFT falls to 35.1% and DPO to 42.9%, both below the 50% random baseline (Table 5, red cells). Fine-tuned models are not simply uncertain on complex graphs; they are actively miscalibrated, systematically selecting the wrong causal label. As $\delta \rightarrow 0$, kernel representations of near-miss pairs become indistinguishable and the decision boundary is determined by surface features that correlate with labels in the training distribution but anti-correlate at higher depths. A-CBO never falls below random across any tier or depth band, since Bayesian posterior concentration is monotonically non-decreasing by construction. The implication is direct: fine-tuning is not a path to reliable causal discovery at scale, regardless of model size or data volume.

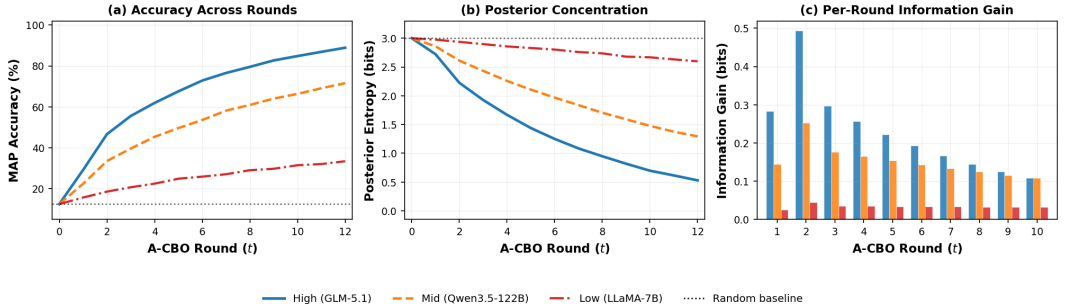


Figure 3: **Convergence over intervention rounds.** Posterior concentration grows monotonically; most models converge within 8–12 rounds well before the budget $T=20$. High-tier models (blue) converge fastest, consistent with lower effective oracle noise η (Theorem 2).

7 CONCLUSION

In this work, we identified a fundamental kernel obstruction that prevents SFT, DPO, and ICL from separating near-miss causal hypotheses, a failure that is geometric and provable, not a matter of model scale or training data. We introduced A-CBO, which escapes this obstruction by relocating the discrete hypothesis decision from the RKHS into an external Bayesian loop over binary interventional queries, and proved convergence in $O(\log n)$ rounds regardless of graph complexity. We also introduced Extended Corr2Cause, a new benchmark covering graphs up to $d=24$ variables, on which A-CBO outperforms the strongest fine-tuned baseline by +26 pp (SFT) and +20 pp (DPO) with *zero training* and the performance gap widens monotonically as graphs scale. Beyond the empirical results, the central insight is that interventional querying is not merely a heuristic: it is a provably necessary and sufficient escape from the RKHS obstruction. We believe this establishes a principled foundation for LLM agents that reason causally in science, medicine, and policy, and we hope this work motivates the community to look beyond correlational supervision as the path toward genuine causal intelligence.

REFERENCES

- A. Abdulaal, hadjivasilou, N. Montana-Brown, T. He, A. Ijishakin, I. Drobnjak, D. C. Castro, and D. C. Alexander Causal Modelling Agents: Causal Graph Discovery through Synergising Metadata and Data-driven Reasoning. In *The Twelfth International Conference on Learning Representations*, 2024. URL <https://openreview.net/forum?id=pAoqRlTBtY>.
- R. Agrawal, C. Squires, K. Yang, K. Shanmugam, and C. Uhler ABCD-Strategy: Budgeted experimental design for targeted causal structure discovery. In *Proceedings of the 22nd International Conference on Artificial Intelligence and Statistics*, pages 3400–3409, 2019.
- H. Chi, H. Li, W. Yang, F. Liu, L. Lan, X. Ren, T. Liu, and B. Han Unveiling causal reasoning in large language models: Reality or mirage?. *Advances in Neural Information Processing Systems*, 37:96640–96670, 2024.
- B. Ghorbani, S. Mei, T. Misiakiewicz, and A. Montanari Limitations of lazy training of two-layers neural network. *Advances in Neural Information Processing Systems*, 32, 2019.
- T. Gupta, W. Gong, C. Ma, N. Pawlowski, A. Hilmkil, M. Scetbon, M. Rigter, A. Famoti, A. J. Llorens, J. Gao, and others The essential role of causality in foundation world models for embodied AI. *arXiv preprint arXiv:2402.06665*, 2024.
- C. Han, Z. Wang, H. Zhao, and H. Ji Explaining emergent in-context learning as kernel regression. *arXiv preprint arXiv:2305.12766*, 2023.
- A. Jacot, F. Gabriel, and C. Hongler Neural tangent kernel: Convergence and generalization in neural networks. *Advances in neural information processing systems*, 31, 2018.
- Z. Jin, J. Liu, Z. Lyu, S. Poff, M. Sachan, R. Mihalcea, M. Diab, and B. Schölkopf Can large language models infer causation from correlation?. *arXiv preprint arXiv:2306.05836*, 2023.
- Z. Jin, Y. Chen, F. Leber, L. Gresele, O. Kamath, B. Xin, Z. Shi, B. Scholkopf, L. Bottou, and R. Mihalcea Cladder: A benchmark to assess causal reasoning capabilities of language models. In *Advances in Neural Information Processing Systems*, 2024.
- K. Kadziolka and S. Salehkaleybar Causal Reasoning in Pieces: Modular In-Context Learning for Causal Discovery. *arXiv preprint arXiv:2507.23488*, 2025.
- D. Karkada The Lazy (NTK) and Rich (μ P) Regimes: A Gentle Tutorial. *arXiv preprint arXiv:2404.19719*, 2024.
- H. D. Le, X. Xia, and Z. Chen Multi-agent causal discovery using large language models. *arXiv preprint arXiv:2407.15073*, 2024.
- J. Li, Y. Chen, C. Liu, Q. Cai, T. Liu, B. Han, K. Zhang, and H. Xiong Can Large Language Models Help Experimental Design for Causal Discovery?. *arXiv preprint arXiv:2503.01139*, 2025.
- H. Li, L. Duan, and Y. Liang Provable In-Context Learning of Nonlinear Regression with Transformers. *arXiv preprint arXiv:2507.20443*, 2025.
- Z. Li and F. Russo Leveraging Large Language Models for Causal Discovery: a Constraint-based, Argumentation-driven Approach. *arXiv preprint arXiv:2602.16481*, 2026.
- N. Scherrer, O. Bilaniuk, Y. Annadani, A. Goyal, P. Schwab, B. Schölkopf, M. C. Mozer, Y. Bengio, S. Bauer, and N. R. Ke Learning neural causal models with active interventions. *arXiv preprint arXiv:2109.02429*, 2021.
- B. Schölkopf, F. Locatello, S. Bauer, N. R. Ke, N. Kalchbrenner, A. Goyal, and Y. Bengio Toward Causal Representation Learning. *Proceedings of the IEEE*, 109(5):612–634, 2021. doi: 10.1109/JPROC.2021.3058954
- E. Sgouritsa, V. Aglietti, Y. W. Teh, A. Doucet, A. Gretton, and S. Chiappa Prompting strategies for enabling large language models to infer causation from correlation. *arXiv preprint arXiv:2412.13952*, 2024.

-
- I. Sheth, B. Fatemi, and M. Fritz Causalgraph2llm: Evaluating llms for causal queries. In *Findings of the Association for Computational Linguistics: NAACL 2025*, pages 2076–2098, 2025.
- H. Sun, A. Jadbabaie, and N. Azizan On the role of transformer feed-forward layers in nonlinear in-context learning. *arXiv preprint arXiv:2501.18187*, 2025.
- W. Sun, J. P. Nogueira, and A. Silva Structured Thinking Matters: Improving LLMs Generalization in Causal Inference Tasks. *arXiv preprint arXiv:2505.18034*, 2025.
- A. Wu, K. Kuang, M. Zhu, Y. Wang, Y. Zheng, K. Han, B. Li, G. Chen, F. Wu, and K. Zhang Causality for large language models. *arXiv preprint arXiv:2410.15319*, 2024.
- X. Wu, K. Yu, J. Wu, and K. C. Tan LLM cannot discover causality, and should be restricted to non-decisional support in causal discovery. *arXiv preprint arXiv:2506.00844*, 2025.
- K. Yamin, S. Gupta, G. R. Ghosal, Z. C. Lipton, and B. Wilder Failure modes of llms for causal reasoning on narratives. *arXiv preprint arXiv:2410.23884*, 2024.
- M. Zečević, M. Willig, D. S. Dhami, and K. Kersting Causal Parrots: Large Language Models May Talk Causality But Are Not Causal. *Transactions on Machine Learning Research*, 2023.
- C. Zhang, S. Bauer, P. Bennett, J. Gao, W. Gong, A. Hilmkil, J. Jennings, C. Ma, T. Minka, N. Pawlowski, and others Understanding causality with large language models: Feasibility and opportunities. *arXiv preprint arXiv:2304.05524*, 2023.

A LIMITATIONS AND FUTURE WORK

A-CBO’s performance ceiling is bounded by oracle fidelity: low-tier models approach random accuracy on large graphs, and the framework assumes the true hypothesis is interventionally distinguishable, a condition that may not hold for all Markov-equivalent DAG classes. The current framework also restricts intervention targets to binary variables and evaluates on synthetically generated premises; extending to continuous interventions, noisy oracles, and real-world text premises remains open. Future directions include relaxing the distinguishability assumption via partial identification, integrating retrieval-augmented generation for automatic premise construction, and exploring active causal discovery settings where the agent jointly selects which variables to intervene on.

B WHY A-CBO CONSTITUTES GENUINE CAUSAL DISCOVERY

Table 1 positions A-CBO against four baselines on dimensions that govern reliability at scale, and a natural question arises: in what sense does any of these methods perform *causal discovery* at all, given that the inputs are textual correlational premises rather than raw data? We answer this question carefully, because the distinction matters for interpreting every row of the table.

What causal discovery requires. Causal discovery is the task of recovering a directed acyclic graph $G = (V, E)$ from evidence about the joint distribution $P(V)$. The foundational difficulty is that observational evidence alone identifies only a *Markov equivalence class* (MEC): a set of DAGs that encode identical conditional independencies and are therefore indistinguishable from passive observation (Schölkopf et al., 2021). Resolving equivalences determining, for instance, whether $A \rightarrow C \rightarrow B$ or $A \leftarrow C \rightarrow B$ generated a given covariance structure requires reasoning about *interventions* and *counterfactuals*. This is the precise sense in which the Corr2Cause task is a causal discovery task: the textual premises encode the full conditional independence structure of the underlying DAG, and the hypothesis to be evaluated is a structural claim about that DAG. The model must go beyond the MEC.

A concrete instance. Consider the following sample from the Corr2Cause dataset Jin et al. (2023)

Premise. Suppose there is a closed system of 4 variables A, B, C , and D . All the statistical relations among these 4 variables are as follows: A correlates with B . A correlates with C . A correlates with D . B correlates with C . B correlates with D . C correlates with D . However, B and D are independent given A . B and D are independent given A and C . C and D are independent given A . C and D are independent given A and B .

Hypothesis. There exists at least one collider (i.e., common effect) of A and B .

Label. 0 (False).

The premise encodes a precise pattern of marginal correlations and conditional independencies. Both a chain $A \rightarrow C \rightarrow D$ with $B \leftarrow A$ and a fork $A \rightarrow C, A \rightarrow D, A \rightarrow B$ are consistent with these statements and crucially, *neither* places a collider on the A - B path. A model that merely memorises surface correlations between hypothesis templates and labels, or that exploits the co-occurrence statistics of “correlates with” and “collider,” will answer incorrectly precisely on instances like this one: the collider template is lexically present (the word appears in the hypothesis), the pairwise correlations are dense (six pairs all correlate), and yet the structural answer is unambiguously negative. Genuine resolution requires reading the conditional independence pattern as a constraint on the set of consistent DAGs, checking whether the hypothesised v-structure ($\cdot \rightarrow B \leftarrow \cdot$) is compatible with any member of that set, and returning the correct verdict.

The methods in Table 1 differ precisely here. Zero-shot prompting and ICL present this reasoning problem to the LLM as a single global prediction. SFT and DPO train the LLM to associate premise-hypothesis pairs with labels. As Theorem 1 proves, all four approaches produce kernel-type predictors whose score margin on near-miss pairs sharing all but a vanishing fraction of their tokens is bounded by $B\kappa\sqrt{2\delta}$, which collapses to zero as graph complexity grows. On the instance above, the distinguishing information (the two conditional independencies $B \perp\!\!\!\perp D \mid A$ and $C \perp\!\!\!\perp D \mid A$ that rule out any v-structure on the A - B path) occupies fewer than five tokens in a premise of over

three hundred. No bounded-norm kernel predictor can amplify a signal of that relative magnitude to a reliable decision margin.

A-CBO escapes this limitation by *never asking the LLM to make this discrimination*. Instead, the Bayesian loop poses a sequence of local interventional queries—“Does D change under $\text{do}(A = v)$?”, “Does C change under $\text{do}(B = v)$?” whose binary answers are kernel-separated by a constant $\rho > 0$ independent of δ (Lemma 2). Each answer eliminates candidate hypotheses: a “yes” to $\text{do}(B)$ affecting C is consistent with a directed path $B \rightarrow \dots \rightarrow C$ but inconsistent with $B \leftarrow A \rightarrow C$ if the path is blocked by the fork. After $T^* = O(\log n / \log \frac{1-\eta}{\eta})$ such queries, the Bayesian posterior concentrates on the surviving DAG class, and the hypothesis is evaluated against it, not by the LLM, but by deterministic graph-mutilation lookup.

The sense in which this is causal discovery. A-CBO recovers the Markov equivalence class (Phase 1) and then resolves equivalences via interventional evidence (Phase 2). This two-phase structure mirrors the classical architecture of causal discovery algorithms such as PC and FCI: constraint-based skeleton recovery followed by orientation via v-structure detection. The difference is that A-CBO’s “experiments” are oracle queries to a frozen LLM rather than physical interventions on a real system. This is legitimate under Assumption 1: if the LLM reliably reports interventional effects (with accuracy $1 - \eta > 1/2$), its answers carry the same logical content as a physical experiment, and the Bayesian update is mathematically equivalent to Bayesian experimental design over the hypothesis space. The discovery is therefore genuine in the formal sense: A-CBO identifies the correct DAG in a process that depends on interventional reasoning, not on correlational pattern matching which is precisely what distinguishes causal discovery from supervised classification.

C EXTENDED RELATED WORK

Causality and LLMs. Schölkopf et al. (2021) posit that genuine causal reasoning requires modelling interventions and counterfactuals, establishing the theoretical gap between pattern recognition and causal inference. Zečević et al. (2023) apply this argument directly to LLMs, introducing meta SCMs to explain why LLMs sometimes appear causal: they recite correlations over causal facts in their training data rather than performing inference, making them “causal parrots.” Wu et al. (2024) move from diagnosis to taxonomy, surveying five distinct stages, from data augmentation to architecture modification, at which causal principles can be integrated into LLMs, and find persistent shortfalls at every stage. Zhang et al. (2023) narrow the question to which specific types of causal queries LLMs can and cannot answer, concluding that they succeed at identifying known causal relations from memorized knowledge but fail at inferring novel ones from statistical evidence. Gupta et al. (2024) argue the problem from the opposite direction: that robust world models must be veridical, faithfully simulating counterfactual consequences rather than pattern-matching, implying that LLMs in their current form cannot serve as causal world models. Concurrently, Wu et al. (2025) argue on empirical and conceptual grounds that LLMs should be restricted to non-decisional support in causal discovery, meaning they should never determine the existence or directionality of causal relationships. While these works converge on the conclusion that LLMs cannot perform genuine causal reasoning, our contribution differs in kind: we prove a formal impossibility showing that the dominant training paradigms cannot overcome this limitation, and we provide a constructive escape that restricts the LLM to exactly the non-decisional oracle role that Wu et al. (2025) advocate.

Benchmarks for causal reasoning in LLMs. Jin et al. (2023; 2024) introduced Corr2Cause, the first benchmark testing pure causal inference from correlational statements, and showed that seventeen LLMs perform near random while fine-tuned models achieve high in-distribution accuracy but collapse under perturbations such as variable renaming or paraphrasing. CausalProbe-2024 (Chi et al., 2024) takes a different approach, using fresh news data unseen during training to distinguish shallow associative reasoning from genuine causal inference, and finds that even state-of-the-art models suffer significant performance drops on novel causal questions, suggesting that strong benchmark performance reflects memorization rather than reasoning. CausalGraph2LLM (Sheth et al., 2025) shifts focus from the reasoning task to the representation problem, evaluating how different graph encoding strategies affect LLM performance on causal tasks and finding high sensitivity to format choices. Yamin et al. (2024) examine a complementary failure mechanism, showing that LLMs rely on superficial heuristics such as event ordering rather than structural reasoning when processing

causal narratives involving chains, forks, and colliders. These benchmarks document the empirical phenomenon our theory explains: degradation that worsens with structural complexity and near-miss configurations. We extend this empirical foundation with Extended Corr2Cause, scaling from 7 to 24 variables with 18K samples, and show that the degradation pattern matches the quantitative predictions of our kernel obstruction theorem.

Prompting and Structured Reasoning for Causal Discovery. Several recent works attempt to improve LLM causal reasoning through better prompting rather than architectural or algorithmic changes. [Sgouritsa et al. \(2024\)](#) propose PC-SubQ, which decomposes Corr2Cause into sub-questions aligned with the steps of the PC algorithm, achieving improved and perturbation-robust performance across five LLMs by guiding the model through each algorithmic step sequentially. [Sun et al. \(2025b\)](#) takes a different approach, introducing explicit DAG construction templates that force the LLM to build the causal structure before answering queries, rather than decomposing the query itself. [Kadziolka and Salehkaleybar \(2025\)](#) combines both ideas, embedding the full PC algorithm within a single unified prompt and evaluating on reasoning-specialist models such as o3-mini and DeepSeek-R1, achieving strong zero-shot baselines without fine-tuning. [Li and Russo \(2026\)](#) go further still, integrating LLM outputs into a formal argumentation framework based on d-separation to ensure logical consistency. While these approaches yield meaningful empirical gains, they all share a structural property: the LLM remains the entity that judges whether a causal relationship holds. Our kernel obstruction theorem implies that this design faces a fundamental ceiling on near-miss hypothesis separation, regardless of how the input is decomposed, because the LLM’s output is still a kernel-type prediction. A-CBO avoids this ceiling by never asking the LLM to distinguish between competing causal graphs. Instead, it poses simple interventional queries whose answers differ across hypotheses, and delegates the discrimination to an external Bayesian loop outside the kernel predictor’s representation space.

LLM-Assisted Causal Discovery with Interventions. LeGIT [Li et al. \(2025a\)](#) introduces a framework in which LLMs propose intervention targets based on their world knowledge about variable semantics, effectively warm-starting numerical causal discovery algorithms when limited interventional data makes gradient-based target selection unreliable. MAC ([Le et al., 2024](#)) explores multi-agent LLM systems for causal discovery, combining a metadata-driven debate module where multiple LLM agents argue about causal relationships with a statistical execution module that validates claims against data. [Abdulaal et al. \(2024\)](#) propose a causal agent which iteratively refines causal graphs by alternating between LLM-proposed structures and deep structural causal model fitting. These methods all use LLMs as *reasoning agents* that make or refine causal judgments, meaning the LLM participates in deciding which edges exist. A-CBO differs in both motivation and mechanism: it is derived from our impossibility theorem, which dictates that the discrete causal decision must reside outside the LLM. The LLM serves only as a fixed oracle answering binary interventional queries, while an external Bayesian loop, operating in the probability simplex rather than the model’s representation space, performs all hypothesis discrimination. LeGIT is closest in spirit, as it also pairs LLMs with an external loop, but it uses the LLM’s domain knowledge to select which interventions to perform, whereas A-CBO uses information-theoretic scoring to select interventions and the LLM only to evaluate their outcomes.

Neural Tangent Kernels, Lazy Training and In-Context Learning. Over-parameterised networks in the lazy/NTK regime produce predictions that evolve as kernel smoothers with fixed feature maps ([Jacot et al., 2018](#)). Recent theoretical work establishes that in-context learning operates within this framework: [Han et al. \(2023\)](#) show that Bayesian inference in ICL can be interpreted as kernel regression over demonstrations, [Sun et al. \(2025a\)](#) prove that transformer blocks with feed-forward layers implement gradient descent on polynomial kernel regression losses, extending the kernel characterisation from linear to nonlinear settings, and [Li et al. \(2025b\)](#) provide the first formal analysis of in-context learning training dynamics for nonlinear regression, showing convergence to kernel-type solutions. Separately, work on the lazy-rich phase transition ([Karkada, 2024](#); [Ghorbani et al., 2019](#)) establishes that the kernel regime and feature learning are mutually exclusive: networks must leave the lazy regime to learn new representations. Our kernel obstruction theorem builds directly on the kernel characterisation of SFT and ICL, deriving a negative consequence that these works do not consider: when two causal hypotheses are observationally near-identical, the kernel representation cannot separate them without the RKHS norm growing unboundedly, violating the conditions that define the lazy regime. A natural question is whether leaving the lazy regime for

the rich/feature-learning regime could resolve the obstruction; A-CBO offers a cheaper escape that preserves the lazy regime entirely.

Causal Bayesian optimisation and active experimental design. Scherrer et al. (2021) introduced active intervention targeting for maximising information gain about causal structure, selecting interventions that most reduce entropy over the hypothesis space. Agrawal et al. (2019) proposed the ABCD-Strategy for budgeted experimental design, providing submodularity-based guarantees on the number of experiments needed to identify the causal graph. Both methods assume access to a physical system where interventions produce real observational outcomes, meaning an experimenter can actually set a variable to a value and measure the downstream effects. A-CBO adapts their information-theoretic framework to a fundamentally different setting where a frozen LLM replaces the physical experiment, answering interventional queries through forward passes rather than data collection. This substitution is justified by our analysis showing that interventional signals remain bounded away from zero even when observational signals collapse, making binary oracle responses sufficient for hypothesis discrimination despite the oracle’s imperfection.

D FULL PROOFS

D.1 PROOF OF LEMMA 1 (NEAR-MISS KERNEL SIMILARITY)

Lemma 3 (Token overlap implies kernel similarity). *Let $\chi^+ = (x, y^+)$ and $\chi^- = (x, y^-)$ share a token prefix of length ℓ out of total sequence length L , with the remaining $L - \ell$ tokens differing. Under the NTK kernel induced by a transformer with bounded Jacobian norms and causal attention, the normalised kernel similarity satisfies:*

$$\frac{K(\chi^+, \chi^-)}{\sqrt{K(\chi^+, \chi^+) \cdot K(\chi^-, \chi^-)}} \geq 1 - C \cdot \frac{L - \ell}{L} \quad (4)$$

for a constant $C > 0$ depending only on κ . Hence $\delta \leq C(L - \ell)/L$.

Proof. Decompose the Jacobian inner product along the token sequence. At each position t , the contribution to $K(\chi^+, \chi^-)$ is:

$$\langle \nabla_{\theta} z_{\theta, t}(\chi^+), \nabla_{\theta} z_{\theta, t}(\chi^-) \rangle.$$

Under causal attention, position t attends only to positions $\leq t$. Consequently:

- At shared positions $t \leq \ell$: inputs are identical so the Jacobians coincide, and each contribution equals $\|\nabla_{\theta} z_{\theta, t}\|^2 \geq 0$.
- At differing positions $t > \ell$: by Cauchy–Schwarz and the diagonal bound $K(\chi, \chi) \leq \kappa^2$, each contribution is bounded below by $-\kappa^2/L$.

Summing over all L positions:

$$K(\chi^+, \chi^-) \geq K(\chi^+, \chi^+) - \frac{2\kappa^2(L - \ell)}{L}. \quad (5)$$

Dividing both sides by $\sqrt{K(\chi^+, \chi^+) \cdot K(\chi^-, \chi^-)}$ and applying $K(\chi^{\pm}, \chi^{\pm}) \leq \kappa^2$ gives:

$$\frac{K(\chi^+, \chi^-)}{\sqrt{K(\chi^+, \chi^+) \cdot K(\chi^-, \chi^-)}} \geq 1 - \frac{2\kappa^2(L - \ell)}{L \cdot K(\chi^+, \chi^+)} \geq 1 - \frac{2(L - \ell)}{L},$$

yielding the stated bound with $C = 2$. \square

Remark. *The positional decomposition assumes approximately uniform Jacobian norm across positions, which is standard in NTK analyses of transformers (Jacot et al., 2018). For near-miss causal instances, $L = O(d^2)$ (the premise contains $O(d^2)$ correlation statements) and $L - \ell = O(1)$ (the reasoning chains diverge only in the final causal inference step), giving $\delta \leq O(1/d^2)$ as claimed in the main text.*

D.2 PROOF OF THEOREM 1 (KERNEL OBSTRUCTION)

Proof of Theorem 1. By Cauchy–Schwarz, $|s(\chi^+) - s(\chi^-)| = |\langle w, \varphi(\chi^+) - \varphi(\chi^-) \rangle| \leq \|w\|_{\mathcal{H}} \cdot \|\varphi(\chi^+) - \varphi(\chi^-)\|_{\mathcal{H}}$.

Expanding:

$$\|\varphi(\chi^+) - \varphi(\chi^-)\|^2 = K(\chi^+, \chi^+) + K(\chi^-, \chi^-) - 2K(\chi^+, \chi^-). \quad (6)$$

Let $a = \sqrt{K(\chi^+, \chi^+)}$, $b = \sqrt{K(\chi^-, \chi^-)}$ with $a, b \leq \kappa$. The δ -similarity gives $K(\chi^+, \chi^-) \geq (1 - \delta)ab$, so:

$$\|\varphi(\chi^+) - \varphi(\chi^-)\|^2 \leq a^2 + b^2 - 2(1 - \delta)ab = (a - b)^2 + 2\delta ab \leq 2\kappa^2\delta. \quad (7)$$

Therefore $|s(\chi^+) - s(\chi^-)| \leq B\kappa\sqrt{2\delta}$. Requiring $\gamma \leq B\kappa\sqrt{2\delta}$ gives $B \geq \gamma/(\kappa\sqrt{2\delta})$. \square

D.3 PROOF OF LEMMA 2 (INTERVENTIONAL KERNEL SEPARATION)

Proof of Lemma 2. Apply Theorem 1 to the interventionally augmented inputs. The bound becomes $B\kappa\sqrt{2\rho}$ where ρ is the interventional sensitivity parameter. The key content is the *decoupling*: ρ depends on the structural difference between hypotheses (via the discrimination set $\mathcal{D}(G^+, G^-)$), while δ depends on observational similarity. Since $(V_i, V_j) \in \mathcal{D}(G^+, G^-)$ is chosen adversarially against the hypotheses, $\rho \not\rightarrow 0$ as $\delta \rightarrow 0$. \square

D.4 PROOF OF THEOREM 2 (CONVERGENCE OF A-CBO)

Proof of Theorem 2. Fix a wrong hypothesis $G_k \neq G^*$. At each round t , the oracle answers correctly with probability $1 - \eta > 1/2$. If the oracle answers correctly:

- If $\hat{r}_k \neq r^{\text{obs}}$: $\pi_k^{(t)} \propto \pi_k^{(t-1)} \cdot \eta$, so π_k is multiplied by $\eta < 1/2$.
- If $\hat{r}_{G^*} = r^{\text{obs}}$: $\pi_{G^*}^{(t)} \propto \pi_{G^*}^{(t-1)} \cdot (1 - \eta)$, so π_{G^*} is multiplied by $(1 - \eta) > 1/2$.

The ratio $\pi_{G^*}^{(t)}/\pi_{G_k}^{(t)}$ grows by a factor of $(1 - \eta)/\eta > 1$ in expectation at each round where the intervention distinguishes G^* from G_k . Since $\mathcal{D}(G^*, G_k) \neq \emptyset$, such an intervention is always available (information gain is positive). After $T^* = \lceil \log n / \log((1 - \eta)/\eta) \rceil$ rounds, for each $k \neq *$:

$$\frac{\pi_{G^*}^{(T^*)}}{\pi_{G_k}^{(T^*)}} \geq \left(\frac{1 - \eta}{\eta} \right)^{T^*} \geq n,$$

with probability at least $1 - \eta^{T^*}$ by a Chernoff-type bound on the Bernoulli oracle. A union bound over all $n - 1$ wrong hypotheses gives success probability $\geq 1 - n\eta^{T^*}$. The algorithm operates only in Δ^{n-1} and never modifies θ_0 , so the lazy/NTK regime is preserved exactly (Proposition 1). The bound T^* depends only on n and η , not on the near-miss parameter δ . \square

D.5 SFT KERNEL DERIVATION

Given input x_u and target $y_u = (y_{u,1}, \dots, y_{u,L})$, SFT minimises:

$$\mathcal{L}_{\text{SFT}}(\theta; x_u, y_u) = - \sum_{l=1}^L \log \pi_{\theta}(y_{u,l} | x_u, y_{u,<l}). \quad (8)$$

The parameter gradient decomposes as:

$$\nabla_{\theta} \mathcal{L}_{\text{SFT}} = \sum_{l=1}^L (\nabla_{\theta} z_{\theta,l})^{\top} (\pi_{\theta}(\cdot | x_u, y_{u,<l}) - e_{y_{u,l}}), \quad (9)$$

where $e_{y_{u,l}}$ is the one-hot vector at token $y_{u,l}$. A first-order Taylor expansion of the effect on a test sequence (x_o, y_o) yields:

$$\Delta \log \pi(y_o | x_o) \approx -\eta \sum_{l,l'} \langle \nabla_{\theta} z_{\theta,l}(x_o, y_{o,<l}), \nabla_{\theta} z_{\theta,l'}(x_u, y_{u,<l'}) \rangle \cdot (\pi_{\theta}(\cdot | x_u, y_{u,<l'}) - e_{y_{u,l'}}), \quad (10)$$

where the inner product of Jacobians is the empirical NTK between the test and training sequences. The resulting predictor is therefore a kernel-type scorer with $\|w\|_{\mathcal{H}}$ controlled by the learning rate η and training duration, confirming $B = O(1)$ under the lazy regime assumption.

E LAZY-PRESERVING PROPERTY OF A-CBO

Proposition 1 (Lazy-Preserving Property of A-CBO). *A-CBO satisfies three properties simultaneously:*

1. **No gradient updates:** the LLM parameters θ_0 are frozen throughout.
2. **Kernel-regime queries:** each LLM call is a standard forward pass; the NTK characterisation applies.
3. **Extra-kernel decision:** the causal judgment is made by the Bayesian posterior update $\pi^{(t+1)} \propto \pi^{(t)} \odot \ell^{(t)}$ in Δ^{n-1} , a space not subject to Theorem 1.

Proof. Items (1) and (2) follow from inspection of Algorithm 1: the only interactions with \mathcal{L} are forward-pass queries. Item (3) holds because the belief update is a deterministic operation on a probability vector performed by the agentic controller. The simplex Δ^{n-1} admits arbitrary discrete concentration without any object in \mathcal{H} changing. \square

A-CBO avoids kernel obstruction entirely by encoding the discrete decision in $\pi \in \Delta^{n-1}$ instead of $w \in \mathcal{H}$. The LLM is used *only for what it can do within the kernel regime* i.e. answering local interventional yes/no questions, not for making global near-miss causal judgments. We summarize this in Appendix F.

F DICHOTOMY SUMMARY

Theorem 1 (negative)	Lemma 2 + Prop. 1 (positive)
Within a bounded-norm kernel predictor, near-miss pairs cannot be separated by more than $B\kappa\sqrt{2\delta}$.	Around a frozen kernel predictor, an agentic loop separates any interventionally distinguishable hypotheses with strength controlled by ρ and η , independently of δ .
Applies to SFT (lazy), DPO, ICL.	Applies to A-CBO with any frozen LLM.
Discrete decision encoded in $w \in \mathcal{H}$.	Discrete decision encoded in $\pi \in \Delta^{n-1}$.
Escape requires leaving the lazy regime.	Lazy regime preserved exactly.

G DETAILED EXPERIMENTAL SETUP

Our Experimental setup: benchmarks, baselines, A-CBO models and hyperparameters, fine-tuning protocol, and evaluation metrics are mentioned in this Table 7

H DATASET STATISTICS

I ADDITIONAL FIGURES

Table 7: Experimental setup: benchmarks, baselines, A-CBO models and hyperparameters, fine-tuning protocol, and evaluation metrics.

Category	Entry	Details
Datasets	CORR2CAUSE	7,524 test samples, $d = 2-6$; six causal relation templates (Parent, Child, Ancestor, Descendant, Collider, Confounder); macro-avg. F1 (Jin et al., 2024).
	EXT. C2C (ours)	18,000 samples, $d = 7-24$ (1K/depth); all-negative labels; binary rejection accuracy; near-miss gap $\propto O(1/d^2)$.
Baselines	Zero-shot GPT-4	Direct prompting, no A-CBO loop; F1 = 29.1.
	LLaMA-7B (FT)	Finetuned on 197,634 in-dist. samples; F1 = 92.0.
	RoBERTa-L SFT	355M params; 1.3M Ext. C2C samples, 3 epochs, AdamW, lr = 2×10^{-5} , batch 32.
	RoBERTa-L DPO	Preference pairs per instance, $\beta = 0.1$; $4 \times A100$.
A-CBO Models	<i>High</i>	GLM-5.1*, Qwen3-30B* (thinking mode enabled)
	<i>Mid</i>	Qwen3.5-122B, Llama-3.3-70B
	<i>Low</i>	Gemma-3-12B-IT, LLaMA-7B
Hyperparameters	Budget / Noise	$T = 20$, $\varepsilon = 0.1$ (random fraction), $\eta = 0.1$ (oracle noise)
	Stopping / Voting	$\delta_c = 0.01$ (entropy threshold), $M = 3$ (majority votes), $N = 8$ (candidates)
Metrics	Orig. / Extended	Macro-avg. F1 over six relation classes / binary rejection accuracy

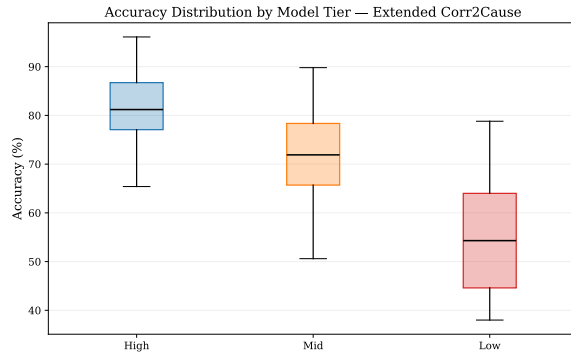


Figure 4: Accuracy distribution by model tier on EXTENDED CORR2CAUSE. Tiers are well-separated with increasing variance at lower tiers (IQR: 8.2 vs. 12.1 vs. 18.6).

Table 8: Statistics of the EXTENDED CORR2CAUSE dataset by graph size d (number of variables). The dataset extends the original Corr2Cause ($d = 2-6$, $\sim 200\text{K}$ samples) to larger causal graphs ($d = 7-28$), totaling over **2.17M** samples. Each graph size contains an equal distribution across all six causal relation templates.

d	# Samples	# Train	# Dev	# Test	# Tok/Premise	% Positive	Vocab
7	12,600	10,600	1,000	1,000	112.0	16.25	65
8	16,800	14,800	1,000	1,000	140.8	19.78	67
9	21,600	19,600	1,000	1,000	173.7	23.48	69
10	27,000	25,000	1,000	1,000	210.9	26.66	71
11	33,000	31,000	1,000	1,000	251.9	29.70	73
12	39,600	37,600	1,000	1,000	297.0	32.60	75
13	46,800	44,800	1,000	1,000	346.0	35.36	77
14	54,600	52,600	1,000	1,000	398.8	37.98	79
15	63,000	61,000	1,000	1,000	456.1	40.46	81
16	72,000	70,000	1,000	1,000	516.9	42.80	83
17	81,600	79,600	1,000	1,000	582.1	45.00	85
18	91,800	89,800	1,000	1,000	650.8	46.00	87
19	102,600	100,600	1,000	1,000	723.8	46.00	89
20	114,000	112,000	1,000	1,000	800.9	46.00	91
21	126,000	124,000	1,000	1,000	882.1	46.00	93
22	138,600	136,600	1,000	1,000	966.9	46.00	95
23	151,800	149,800	1,000	1,000	1,055.9	46.00	97
24	165,600	163,600	1,000	1,000	1,148.9	46.00	99
25	180,000	180,000 [†]	—	—	1,246.0	46.00	101
26	195,000	195,000 [†]	—	—	1,347.2	46.00	103
27	210,600	210,600 [†]	—	—	1,452.5	46.00	105
28	226,800	226,800 [†]	—	—	1,561.9	46.00	107
All	2,171,400	2,135,400	18,000	18,000	991.5	38.64	107

Tok/Hypothesis is constant at 8.7 across all d (omitted for brevity). All six causal templates (parent, child, non-parent ancestor, non-child descendant, has_collider, has_confounder) are uniformly distributed ($\frac{1}{6}$ each).

[†] $d = 25-28$ provided as raw JSON with full graph metadata; no pre-split Dev/Test partition.

Small ($d=7-10$)
Medium ($d=11-15$)
Large ($d=16-20$)
XL ($d=21-24$)
Extended ($d=25-28$)